Dual-Energy CT: Spectrum of Thoracic Abnormalities[1]

Alexi Otrakji, MD
Subba R. Digumarthy, MD
Roberto Lo Gullo, MD
Efren J. Flores, MD
Jo-Anne O. Shepard, MD
Mannudeep K. Kalra, MD

Abbreviations: PBV = pulmonary blood volume, VNC = virtual unenhanced

RadioGraphics 2016; 36:38–52

Published online 10.1148/rg.2016150081

Content Codes: CH CT PH VA

[1]From the Division of Thoracic Imaging, Department of Radiology, Massachusetts General Hospital, Harvard Medical School, 55 Fruit St, Founders 213, Boston, MA 02114. Presented as an education exhibit at the 2014 RSNA Annual Meeting. Received March 24, 2015; revision requested April 24 and received May 22; accepted July 31. For this journal-based SA-CME activity, the authors, editor, and reviewers have disclosed no relevant relationships. **Address correspondence to** A.O. (e-mail: *aotrakji@partners.org*).

SA-CME LEARNING OBJECTIVES

After completing this journal-based SA-CME activity, participants will be able to:

- List the principles of dual-energy CT, including its acquisition and postprocessing techniques.
- Appraise the utility of the use of monochromatic and virtual unenhanced images.
- Explain the importance of simultaneous interpretation of pulmonary blood volume and lung-window images.

See www.rsna.org/education/search/RG

Recent studies have demonstrated that dual-energy computed tomography (CT) can provide useful information in several chest-related clinical indications. Compared with single-energy CT, dual-energy CT of the chest is feasible with the use of a radiation-dose-neutral scanning protocol. This article highlights the different types of images that can be generated by using dual-energy CT protocols such as virtual monochromatic, virtual unenhanced (ie, water), and pulmonary blood volume (ie, iodine) images. The physical basis of dual-energy CT and material decomposition are explained. The advantages of the use of virtual low-monochromatic images include reduced volume of intravenous contrast material and improved contrast resolution of images. The use of virtual high-monochromatic images can reduce beam hardening and contrast streak artifacts. The pulmonary blood volume images can help differentiate various parenchymal abnormalities, such as infarcts, atelectasis, and pneumonias, as well as airway abnormalities. The pulmonary blood volume images allow quantitative and qualitative assessment of iodine distribution. The estimation of iodine concentration (quantitative assessment) provides objective analysis of enhancement. The advantages of virtual unenhanced images include differentiation of calcifications, talc, and enhanced thoracic structures. Dual-energy CT has applications in oncologic imaging, including diagnosis of thoracic masses, treatment planning, and assessment of response to treatment. Understanding the concept of dual-energy CT and its clinical application in the chest are the goals of this article.

Introduction

The concept of the use of multiple energy levels in computed tomography (CT) was first initiated 40 years ago, but a lack of appropriate technology did not allow clinical implementation (1). Recent advances in technology have resolved many challenges related to the implementation of dual-energy CT techniques and image acquisition (2,3). Dual-energy CT refers to the near-simultaneous acquisition of CT images at two x-ray energy levels. Concerns over increased radiation dose with dual-energy CT were an impediment to the adoption of this technique, but the use of modern scanners, especially those that with tube current modulation, have resolved this concern. Use of dual-energy CT in the chest can help with the evaluation of several chest abnormalities, such as pulmonary embolism, other vascular abnormalities, thoracic malignancies, interstitial lung disease, and mediastinal abnormalities (2).

TEACHING POINTS

- Near-simultaneous imaging at high and low kilovoltages, as occurs with most dual-energy CT–capable scanners, provides an optimal combination of the greater photoelectric absorption afforded by low voltage and lower image noise afforded by high voltage.
- The use of low-kilovoltage monochromatic dual-energy CT images can increase the enhancement of the pulmonary arteries when arterial enhancement is suboptimal on single-energy images, which leads to improved confidence in interpretation of CT pulmonary angiography images compared with conventional (single-energy) CT pulmonary angiography and a higher voltage (100–140 kV), in which it is not possible to improve image contrast.
- Low virtual monochromatic images (≤ 60 keV) can provide optimal, diagnostic enhancement of the pulmonary arteries for a diagnosis of pulmonary embolism with a reduced volume of contrast material.
- The ideal way to differentiate between iodine distribution defects is to use an approach for PBV images or iodine maps similar to that used for ventilation-perfusion images, in which the mismatch between ventilation-perfusion images is essential to diagnose pulmonary embolism.
- Consequently, creation of higher-monochromatic images can help troubleshoot artifacts related to large patient size and placement of arms by the side of the body.

Fundamentals of Dual-Energy CT

Physical Basis

Applied tube potential, which is expressed in kilovolts, determines the peak energy of x-ray photons (4). At high kilovoltage, Compton scatter is the prevailing interaction of x-ray photons with the body tissues. Compton scatter is independent of the characteristics of the tissues or materials with which the x-ray photons interact. On the other hand, photoelectric absorption of x-ray photons increases as photon energy (eg, low kilovoltage) decreases. This phenomenon is closely linked to the atomic number, *(Z)* of materials or tissues. While single-energy low-kilovoltage imaging has greater photoelectric absorption, it also has higher image noise (5). Near-simultaneous imaging at high and low kilovoltages, as occurs with most dual-energy CT–capable scanners, allows an optimal combination of the greater photoelectric absorption afforded by low kilovoltage and less image noise afforded by high kilovoltage.

Photoelectric Interactions and Material Decomposition in Dual-Energy CT

Single-energy CT provides information on the x-ray attenuation coefficient (measured in Hounsfield units) at one energy level. However, when dual x-ray energies (ie, dual-energy CT) are used, additional information on two physical quantities can be obtained, a feature also known as atomic number and electron density of the two base materials. In the diagnostic range of x-ray energy (which is generally 10–150 keV), interactions between the tissues and x-rays result in photoelectric absorption and Compton scatter. Photoelectric absorption refers to the transfer of x-ray energy to an atom, with resultant emission of characteristic radiation, which is dependent on two key material-specific parameters: effective atomic number and electron density. Photoelectric absorption with specific material occurs when the x-ray photon energy equals or slightly exceeds its k-shell electron binding energy (known as the k-edge).

Compton scattering is the predominant interaction in which x-ray photons transfer some energy to an electron and change their direction. While Compton scattering is proportional to the electron density, photoelectron absorption is directly proportional to both atomic number and electron density. Compton scattering is predominant at higher x-ray energy levels, whereas photoelectric absorption is much higher at the lower x-ray energy levels. Thus, iodine ($Z = 53$) is more attenuating than calcium ($Z = 20$), and calcium is more attenuating than organic compounds such as water (2,5). The differential interactions of two x-ray energies form the physical basis for the decomposition of images into two base materials (eg, water and calcium, calcium and iodine, and iodine and water) as long as their atomic numbers are different. Body soft tissues with a predominant water component can be decomposed from bones, which have a substantial calcium component. Likewise, at contrast material–enhanced CT, images can be decomposed to separate regions of iodine uptake from soft tissues that do not demonstrate uptake and have a much lower atomic number to obtain iodine- (subtracting waterlike soft tissues from iodine) or water- (subtracting iodine from the waterlike soft tissues) attenuation images.

Dual-Energy CT Techniques

To obtain dual-energy CT images, many modifications were made to the capabilities available with multidetector CT (2). There are four available methods for acquiring dual-energy CT images, the first of which involves the use of dual x-ray sources (Siemens Healthcare, Forchheim, Germany), with two perpendicular x-ray tubes (one with high kilovoltage, and one with low kilovoltage) and separate detectors. Each tube has the ability to simultaneously operate at two different kilovoltages: 70–100 kV for the low-kilovoltage setting and 140 –150 kV for the high-kilovoltage setting (Fig 1) (6). Dual-source CT allows the use of an automatic exposure control technique (CARE dose 4D; Siemens) to enable dose modulation. On the other hand,

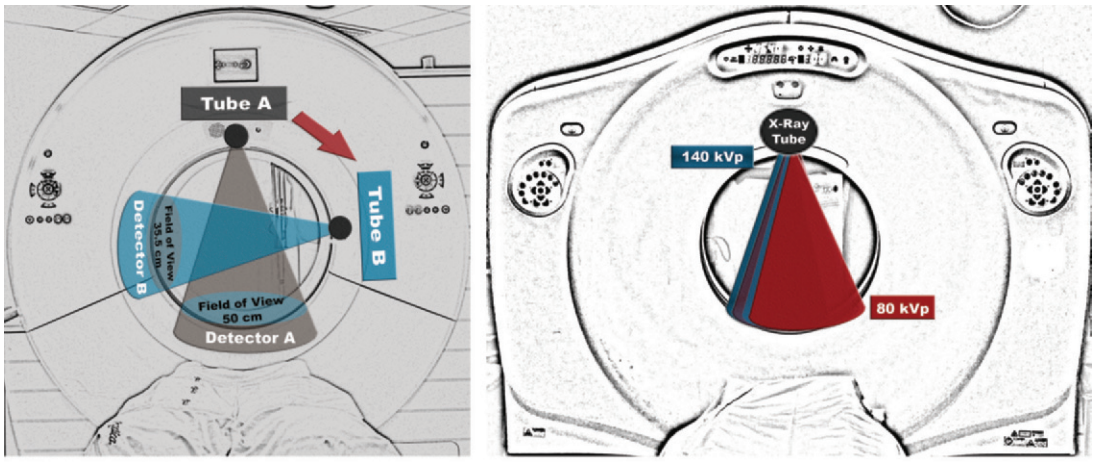

Figure 1. **(a)** Diagram shows a dual-source dual-energy CT scanner, with two x-ray tubes and two detector panels with which to simultaneously acquire dual-energy CT images. For the third-generation dual-source CT scanners, the field of view of the low-kilovoltage tube is limited to 35.5 cm. **(b)** Diagram shows a single x-ray-source scanner, which acquires two kilovoltage data sets during the same acquisition by rapidly switching between low and high kilovoltages (80–140 kV).

Table 1: Main Differences between the Three Generations of Dual-Source Dual-Energy CT Systems

Parameter	1st Generation	2nd Generation	3rd Generation
Field of view (cm)*	26	33	35.5
Detector configuration (mm)	32.0 × 0.625	64.0 × 0.625	96.0 × 0.6
Imaging speed (mm/s)	430	458	737
No. of acquired sections†	128 (2 × 64)	256 (2 × 128)	384 (2 × 192)
Limits (kV)	80–140	80–140	70–150
Rotation time (sec)	Up to 0.33	Up to 0.28	Up to 0.25
Iterative reconstruction‡	IRIS	SAFIRE	ADMIRE

Source.—Referenced 3.
*For the low-energy tube.
†Data are total number of sections, and data in parentheses are number of rows × number of sections.
‡ADMIRE = advanced modeled iterative reconstruction, IRIS = iterative reconstruction in image space, SAFIRE = sonogram-affirmed iterative reconstruction.

dual-source CT allows the use of multiple kilovoltage combinations (ie, 70–100 kV and 140–150 kV). A limitation of the use of dual-source CT is its limited field of view of up to 35.5 cm, which necessitates careful patient centering. There are three generations of dual-source dual-energy CT scanners (Table 1).

The second acquisition method involves a rapid kilovoltage-switching technique (GE Healthcare, Milwaukee, Wis), in which a single x-ray tube rapidly (0.5 msec) switches the tube energy from 80 to 140 kV during the same tube rotation (Fig 1). These scanners are equipped with gemstone detectors, which allow rapid recording of the different-energy x-rays. They allow a 50-cm field of view at 64 × 0.625-mm detector configuration and a fixed energy of 80–140 kV. On the other hand, this technology does not permit the use of automatic exposure control and, therefore, may be associated with higher radiation dose than single-energy CT. The use of adaptive statistical iterative reconstruction is available for dual-energy image reconstruction (7).

The third method uses a separate rotation (spin) technique (Toshiba, Tochigi, Japan), which involves initial data acquisition at a low kilovoltage and a subsequent x-ray tube rotation to acquire data at a high kilovoltage with a single tube (8). Adaptive iterative dose reduction is used to reduce noise. An inability to acquire near-simultaneous dual-energy CT data sets limits its application in the chest, particularly for dynamic contrast-enhanced CT.

The fourth method was developed on the basis of a sandwich detector (Philips Healthcare, Eindhoven, the Netherlands), which uses a dual layer of detectors to generate spectral information, with the superficial layer absorbing lower-energy

Table 2: Commercially Available Dual-Energy CT Techniques

Scanner Type	Advantages	Disadvantages
Dual source	AEC possible, two image data sets at low and high kilovoltages	Limited field of view (26–35.5 cm) for low-energy tube, asynchronous projection
Single source	Matched image processing based on projection methods, 50-cm field of view	AEC not possible, radiation dose can be higher than at single-energy CT
Dual rotation (spin)	Cost effective, AEC possible	Misregistration between low- and high-kilovoltage data sets due to temporal separation
Dual layer	AEC available, synchronous projection	Same filtration used for both to low- and high-energy

Sources.—References 1 and 8.
Note.—AEC = automatic exposure control

x-ray photons and the deeper layer absorbing higher-energy photons (6). Dual-layer detector scanners use iterative model reconstruction to reduce image noise.

A novel method, which is still experimental, uses photon-counting detectors to separate x-ray photons according to their energies (8). In our department, all images were obtained with either single-source (Discovery CT750 HD; GE Healthcare) or dual-source (Somatom Definition Flash and Somatom Force; Siemens) dual-energy CT (Table 2).

Image Postprocessing

There are considerable variations in image processing with the dual-energy CT data sets. Dual-source CT scanners generate separate low- and high-kilovoltage image series and a weighted, blended data set that combines information from the low- and high-kilovoltage images. These image data sets can be used to generate additional virtual monochromatic and material decomposition images, depending on which image-based method is used (1).

Rapid kilovoltage-switching scanners generate a quality check data set that is, basically, the high kilovoltage data set. Users can reconstruct virtual monochromatic images by using image projection data. Some virtual monochromatic image files can then be uploaded to offline workstations to generate other monochromatic and material decomposition images.

Virtual monochromatic images can be generated within a spectral range of 40–190 keV for dual-source CT and 40–140 keV for single-source CT. Image series with a lower kilovoltage have higher contrast (ie, closer to the k-edge of iodine) and more noise, a result of lower energy. High monochromatic images have less noise and fewer streak artifacts, but they also have lower image contrast, particularly on contrast-enhanced CT images. To reduce noise and decrease the number of artifacts in low-kilovoltage images, monochromatic plus images (syngo.via; Siemens Healthcare)—a blending option for monochromatic images that combines the rich contrast information of low-kilovoltage data sets with low noise information from high-kilovoltage data sets—were recently released for the dual-source scanner (9). At our institution, we use 60-keV and monochromatic plus 40-keV images for chest dual-energy CT.

Material decomposition images refer to three material decomposition (ie, iodine, calcium, and water) capabilities of the dual-energy CT data sets, in which users can subtract one material type from the other. For example, virtual unenhanced (VNC), or water, images can be generated from contrast-enhanced dual-energy CT data sets by subtracting the iodine from the water component. These VNC images allow for differentiation of calcification or high-attenuation materials (eg, calcium, talc) from iodine-enhanced tissues. Likewise, iodine, or blood volume, images can be generated by subtracting water from contrast-enhanced CT data sets. These images allow better qualitative and quantitative evaluation of iodine enhancement in tissues and lesions than do conventional single-energy CT images. Furthermore, these decomposition images allow measurement of absolute water and iodine content in the region of interest (Table 3).

There are some key differences between dual-energy and single-energy CT. Because of the limited field of view with dual-source dual-energy CT, it is important to carefully center patients so that the anatomic region of interest for dual-energy CT is included in the field of view. Dual-source dual-energy CT allows the use of up to a 0.28-sec rotation time, whereas 0.5 second is the minimum achievable rotation time for kilovoltage-switching dual-energy CT. Both the amount of contrast material and the rate of injection can be slowed for chest dual-energy CT compared

Table 3: Summary of Dual-Energy CT Image Types

Image Type	Description
Blended (Siemens Healthcare)	Blend of low and high kilovoltages
Quality check (GE Healthcare)	Unblended high kilovoltage
Virtual monochromatic*	High monochrome, with less noise and fewer artifacts
Material decomposition†	
VNC or water	Represents iodine subtraction, helps to determine extent of enhancement and to differentiate calcium and talc from iodine
PBV or iodine	Represents water subtraction, allows quantification of iodine distribution and lung perfusion

*At 40–190 keV.
†PBV = pulmonary blood volume.

with those for single-energy CT because of the increased sensitivity of iodine in low-kilovoltage images. Another practical difference is that the number of image series and images generated with dual-energy CT are much greater than those generated with single-energy CT.

To maximize efficient interpretation of dual-energy CT images, we recommend that radiologists begin their interpretation with a review of 40- or 60-keV monochromatic images with lung (window width, 1500 HU; window level, −600 HU) and mediastinal (window width, 400 HU; window level, 40 HU) settings. Because of the increased contrast enhancement in low-kilovoltage images, radiologists should widen mediastinal windows to assess vascular structures (eg, emboli, dissection flaps, and plaques) on the basis of contrast enhancement. Subsequently, radiologists should simultaneously display these monochromatic images at lung window settings with material decomposition images to assess iodine enhancement (on pulmonary blood volume or iodine images) or a lack of enhancement (VNC images). With experience, a review of dual-energy CT images takes no more than a few additional seconds per case.

Radiation Dose

Radiation dose is an important consideration with regard to CT because of concerns about an associated risk for radiation-induced carcinogenesis (10). Many factors play a role in determining the radiation dose in dual-energy CT, such as automatic exposure control, applied low and high kilovoltage, imaging length, and iterative reconstructions (11). Dual-source (first and second generation) dual-energy pulmonary CT angiography has been reported as being dose neutral compared with single-energy CT protocols performed with the same scanner. By performing dual-energy CT at 80 and at 140 kV with a tin filter, the difference in CT dose index is greater than 1 mGy, making the dose lower with dual-energy CT (12). The ability to produce VNC images with dual-energy CT can provide information similar to that obtained with real unenhanced CT and adds another opportunity to decrease the radiation dose in multiphasic CT examinations, such as CT angiography for evaluation of the thoracic aorta (13). With the rapid kilovolt-switching technique, radiation dose of dual-energy CT can be higher than that of single-energy CT.

Clinical Applications

Vascular Abnormalities

One of the main applications of chest dual-energy CT is the evaluation of pulmonary embolism. Making an accurate diagnosis of pulmonary embolism requires optimal pulmonary enhancement triggered with bolus-tracking techniques. The use of low-energy monochromatic dual-energy CT images can increase the enhancement of the pulmonary arteries when arterial enhancement is suboptimal on single-energy images, which leads to improved confidence in interpretation of CT pulmonary angiography images compared with conventional (single-energy) CT pulmonary angiography and a higher kilovoltage (100–140 kV), in which it is not possible to improve image contrast (14). Low-energy virtual monochromatic images (≤ 60 keV) are acquired with dual-energy CT pulmonary angiography to ensure high attenuation in pulmonary vessels, even to the level of subsegmental vessels.

Because of the risk for contrast material–induced nephropathy, contrast-enhanced CT with a full contrast agent dose (≥ 70 mL) may not be possible in patients with compromised renal function and an estimated glomerular filtration rate (eGFR) of less than 30 mL/min/1.73 m^2 or when there is a need to repeat CT pulmonary angiography a short time (< 24 hours) after undergoing an intravenous contrast-enhanced

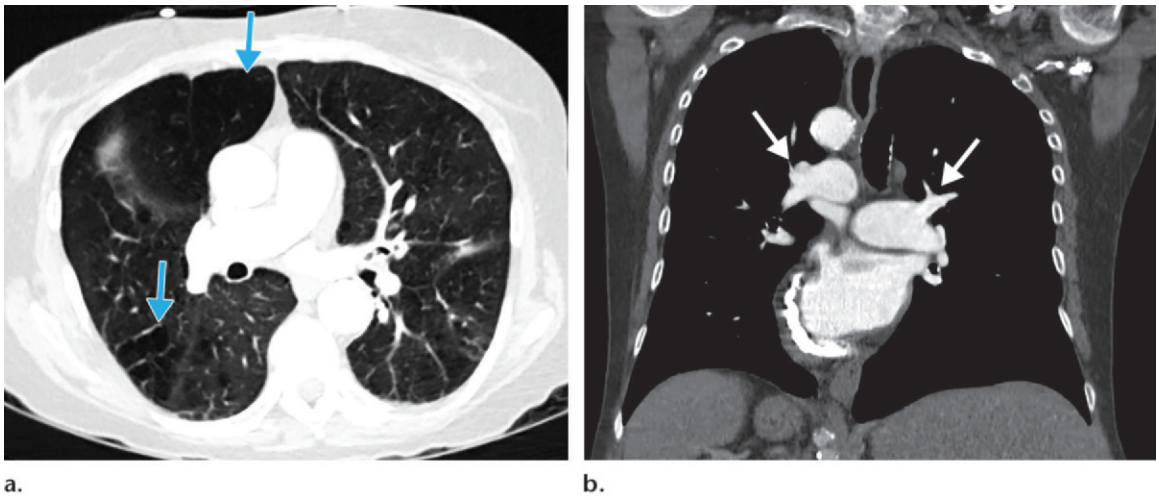

a. b.

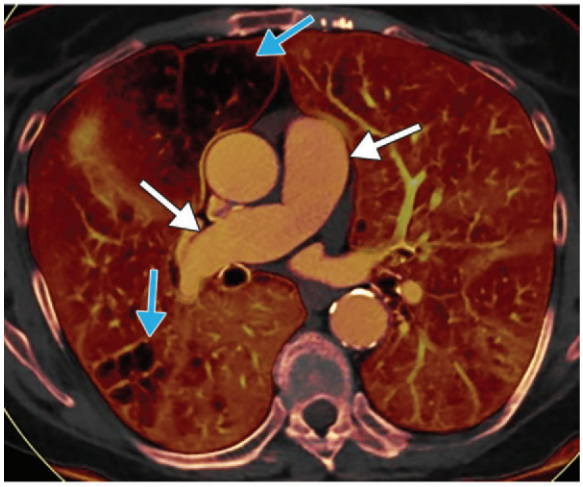

c.

Figure 2. Emphysema in a 63-year-old woman who weighed 54 kg, had a recent history of renal transplantation (eGFR, 42 mL/min/1.73 m2), and presented with acute-onset shortness of breath. Chest radiograph (not shown) depicted emphysema and patchy bilateral pulmonary opacities that could have compromised the yield of nuclear medicine ventilation-perfusion imaging. The patient underwent dual-energy CT pulmonary angiography with 25 mL of contrast material (routinely, 80 mL injected). **(a)** Transverse CT image obtained at 60 keV shows scattered emphysema (arrows) in both lungs. **(b)** Coronal CT image obtained at 60 keV shows excellent vascular enhancement of the pulmonary arteries (arrows), with attenuation of 314 HU in the main pulmonary artery. **(c)** Transverse PBV image shows excellent enhancement in the pulmonary arteries (white arrows) and scattered dark areas without iodine distribution (blue arrows), which correspond to emphysema.

examination (15). Low virtual monochromatic images (≤ 60 keV) can provide optimal, diagnostic enhancement of the pulmonary arteries for a diagnosis of pulmonary embolism with a reduced volume of contrast material (16). Patients with an intermediate risk for contrast material–induced nephropathy (eGFR, 30–60 mL/min/1.73 m^2) can undergo CT pulmonary angiography with only 25–35 mL of iodinated contrast material (iodine concentration, 370 mg/mL) (Fig 2).

The use of multiple phases of contrast material injection in dual-source dual-energy CT pulmonary angiography was reported by Kerl et al (17). They found that optimal enhancement in pulmonary arteries and fewer contrast material–related streak artifacts from the subclavian vein and superior vena cava occurred when three boluses were administered: 50 mL of contrast material (400 mg%), a 30-mL solution of 30% contrast material and 70% sodium chloride (NaCl) saline, and 50 mL of NaCl saline.

Material decomposition images in dual-energy CT, such as iodine maps and PBV images, provide additional information about pulmonary perfusion by assessing iodine distribution in the lungs. PBV images have the potential to depict defects in iodine distribution as a result of several pulmonary abnormalities (18,19). The ideal way to differentiate between iodine distribution defects is to use an approach for PBV images or iodine maps similar to that used for ventilation-perfusion scans, in which the mismatch between ventilation-perfusion scans is essential to diagnosing pulmonary embolism (20). In the case of chest dual-energy CT, correlating findings between PBV images or iodine maps, which resemble perfusion images, and conventional lung attenuation on dual-energy CT images, which resemble ventilation images, is the key to narrowing the differential diagnosis for iodine distribution defects. On PBV images, pulmonary embolism–related defects have characteristic features in pulmonary infarction and pulmonary embolism without infarction. In infarction, there is a peripheral wedge-shaped area of nonenhancement that is usually bigger than the pulmonary opacity seen on images obtained with lung window settings. In pulmonary occlusive vascular diseases without infarction, areas of decreased attenuation are seen on PBV images, with no corresponding opacity on CT images obtained with lung window

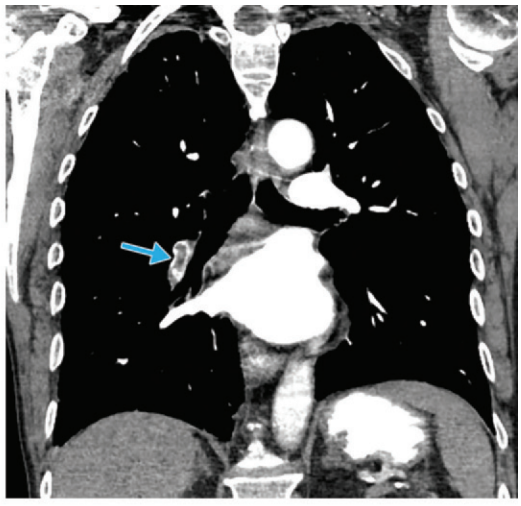

a.

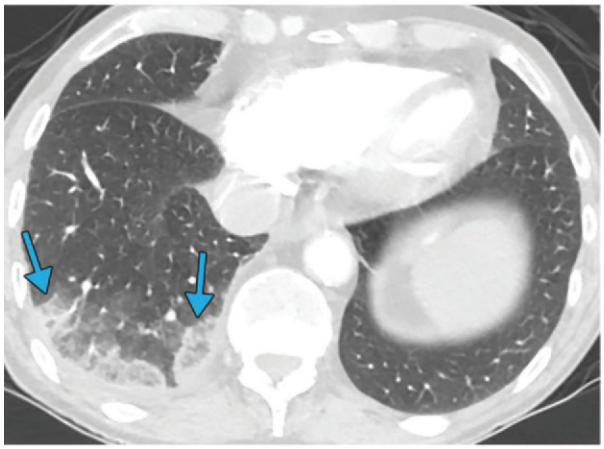

b.

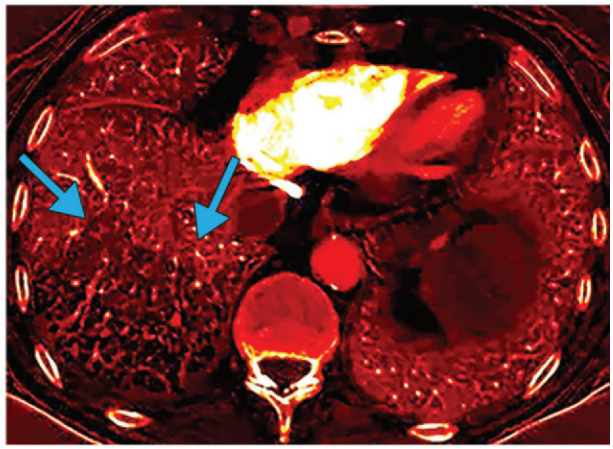

c.

Figure 3. **(a)** Coronal CT image obtained at 60 keV shows a filling defect in the right interlobar artery (arrow). **(b)** Transverse CT image obtained at 60 keV with lung window settings shows wedge-shaped opacities in the right lower lobe with surrounding ground-glass opacities (arrows). **(c)** Transverse PBV image shows a homogeneous subpleural area of decreased PBV (arrows) in the right lower lobe. This area is larger than the corresponding opacities seen on **a** and **b.** The mismatch between PBV and findings on **a** and **b** likely represents a pulmonary infarct.

settings. In acute infarction, the size of the opacity on conventional CT images obtained with lung window settings is smaller than area of decreased blood volume on PBV images (Fig 3). PBV images are very sensitive to decreased iodine content in lungs, a finding that may not be apparent on conventional CT images (Fig 4). The high sensitivity of PBV images for depicting subtle decreases in iodine content circulation allows identification of small pulmonary emboli by careful, retrospective evaluation of pulmonary arteries.

Pulmonary hypertension resulting from chronic thromboembolic pulmonary disease is associated with substantial morbidity and mortality (21). Conventionally, catheterization of the right side of the heart, with pulmonary arteriography and ventilation-perfusion scanning, is performed for preoperative workup. The potential of dual-energy CT pulmonary angiography for evaluating patients suspected of having pulmonary embolism and pulmonary arterial hypertension was reported in the literature (22). Dournes et al (23) reported that dual-energy CT perfusion had 100% sensitivity and 92% specificity, which is superior to the diagnostic performance of scintigraphy for depicting chronic thromboembolic pulmonary hypertension, in 40 patients with proved pulmonary hypertension. Dual-source dual-energy CT (syngo.via; Siemens) enables quantification of lung parenchymal enhancement in any desired portion of the lung by drawing a region of interest. Enhancement in the upper, middle, and lower thirds of the lung can also be assessed similar to the way it is assessed at perfusion imaging in nuclear medicine (Fig 5). The peripheral decrease in lung parenchymal enhancement with increased enhancement of the main pulmonary artery was reported by Ameli-Renani et al (24) in patients with pulmonary artery hypertension.

The depiction of pulmonary embolism is not the only vascular application of dual-energy chest CT. The use of low monochromatic images increases enhancement of the systemic vasculature, as well as the pulmonary arteries. Hence, there are fewer opportunities to miss incidental aortic abnormalities, such as aortic dissection, compared with suboptimal aortic enhancement at CT pulmonary angiography or routine chest ex-

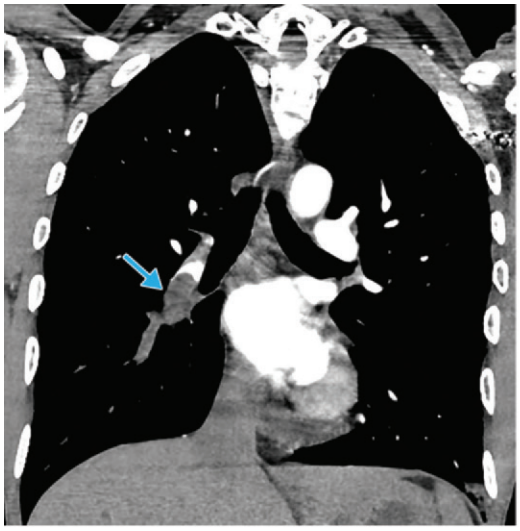

a.

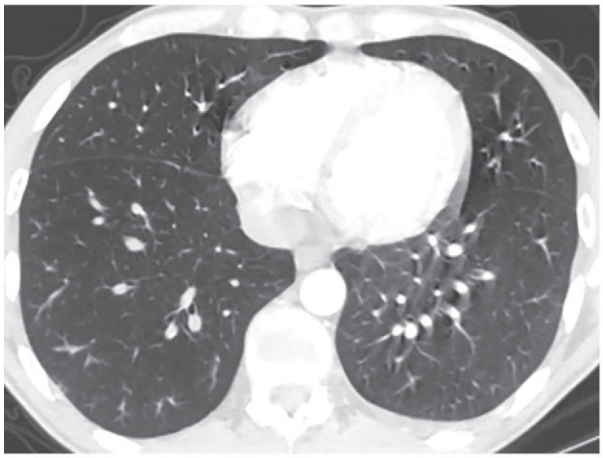

b.

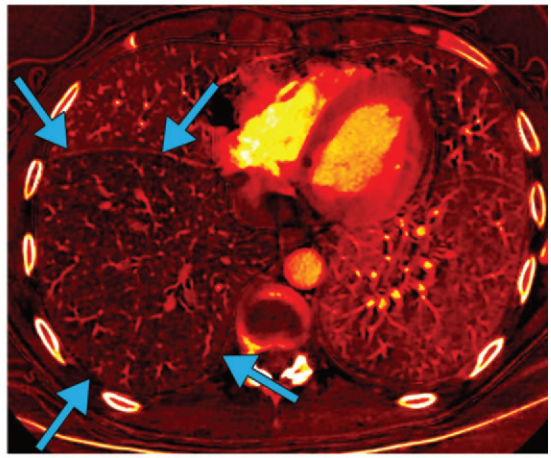

c.

Figure 4. **(a)** Coronal CT image obtained at 60 keV shows a large occlusive filling defect in the right interlobar artery that extends into the distal pulmonary arteries in the right lower lobe (arrow). **(b)** Transverse CT image obtained at 60 keV shows no substantial lung abnormality in the right lower lobe. **(c)** Transverse PBV image shows a large area of decreased pulmonary blood volume in the entire right lower lobe (arrows), a finding consistent with pulmonary embolism–induced decreased circulation in the lobe.

amination. Furthermore, material decomposition dual-energy CT images can help differentiate between the several aortic diseases (25). For example, VNC imaging has the capability to replace true unenhanced CT for depiction and follow-up of real endoleaks after aortic aneurysm repair (26,27). On the other hand, PBV images depict intense iodine distribution in vasculature and in vascular malformations. Dual-energy CT pulmonary angiography can better depict and facilitate evaluation of arteriovenous malformations, and thin (1. 5 × 1. 5 mm) coronal and axial PBV images are useful for depicting small arteriovenous malformations and their nidi (Fig 6).

Lung Malignancies

Initial evidence for the use of dual-energy CT in patients with thoracic malignancies was reported in small sample studies. Iodine concentration measurement from material decomposition images in evaluation of thoracic malignancies has the potential to differentiate between benign and malignant tumors. Previous studies reported substantial differences in iodine concentrations in early and delayed phases between benign and malignant mediastinal neoplasms, but no difference was noted in their CT attenuation numbers (28). In a study of 37 patients with non–small cell lung cancer, there was good correlation between iodine concentration at dual-energy CT and fluorodeoxyglucose uptake (29). In a recent study on dual-phase dual-energy CT protocols (unenhanced and 3 minutes after administration of contrast material) in 49 patients with indeterminate pulmonary nodules, Chae et al (30) reported that malignant nodules showed significantly greater contrast enhancement at 3 minutes than did benign nodules ($P = .001$). In addition, VNC images depicted most of the calcifications in pulmonary nodules and lymph nodes that were seen on true unenhanced images. Small foci of calcifications can be missed on VNC or water images obtained from dual-energy CT data sets (31). Given the importance of characterization of incidental pulmonary nodules in the view of interest at lung cancer screening CT, larger prospective studies are necessary to explore applications

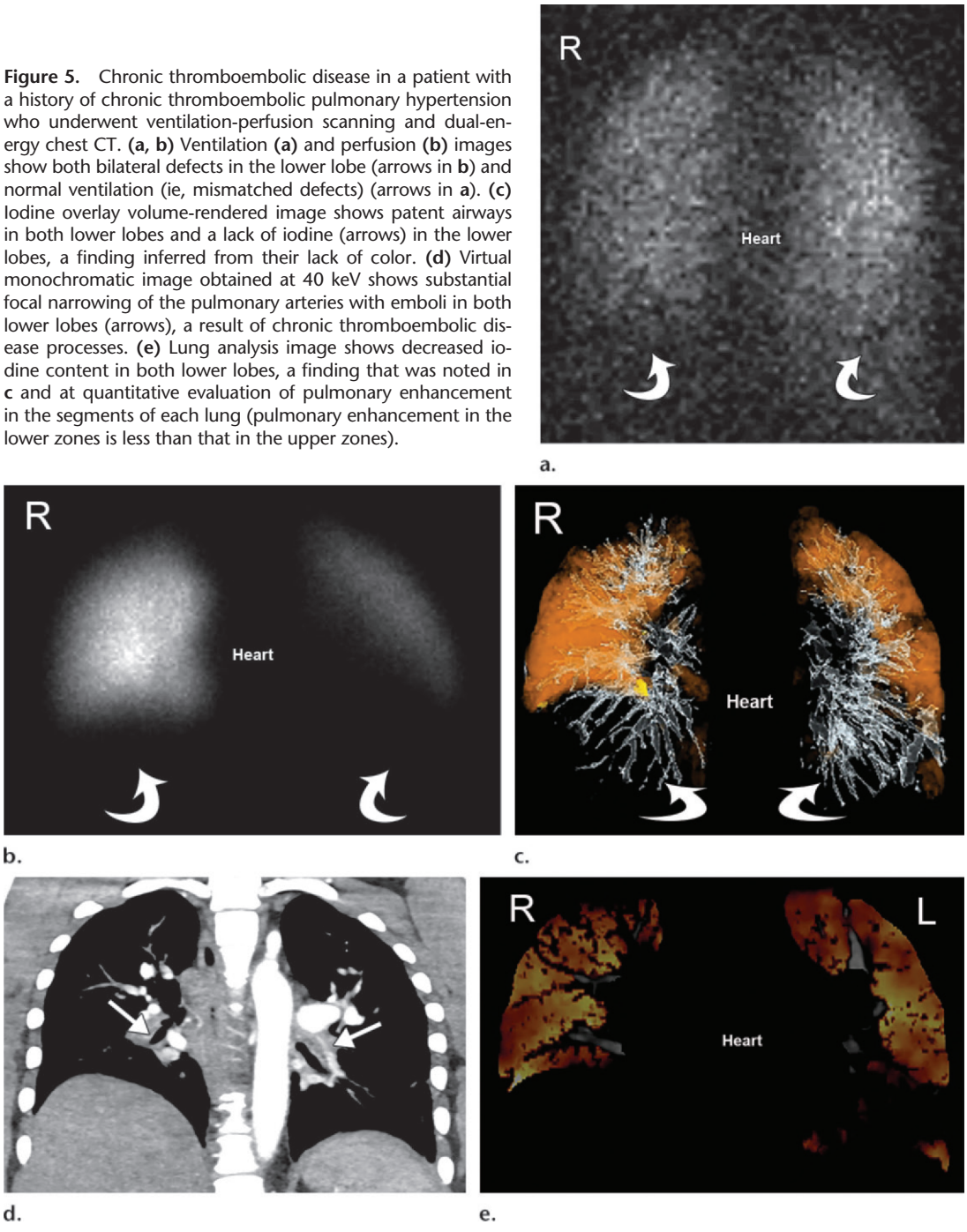

Figure 5. Chronic thromboembolic disease in a patient with a history of chronic thromboembolic pulmonary hypertension who underwent ventilation-perfusion scanning and dual-energy chest CT. **(a, b)** Ventilation **(a)** and perfusion **(b)** images show both bilateral defects in the lower lobe (arrows in **b**) and normal ventilation (ie, mismatched defects) (arrows in **a**). **(c)** Iodine overlay volume-rendered image shows patent airways in both lower lobes and a lack of iodine (arrows) in the lower lobes, a finding inferred from their lack of color. **(d)** Virtual monochromatic image obtained at 40 keV shows substantial focal narrowing of the pulmonary arteries with emboli in both lower lobes (arrows), a result of chronic thromboembolic disease processes. **(e)** Lung analysis image shows decreased iodine content in both lower lobes, a finding that was noted in **c** and at quantitative evaluation of pulmonary enhancement in the segments of each lung (pulmonary enhancement in the lower zones is less than that in the upper zones).

of VNC images in depicting the tiny calcifications of nodules on contrast-enhanced dual-energy CT images of the chest. Another advantage of VNC images is that they may replace true unenhanced CT in the evaluation of lymph nodes. Yang et al (32) found that for the same cervical lymph nodes, there were no big differences (about 8 HU) in CT attenuation values between VNC and true unenhanced CT at dual-source dual-energy CT.

Furthermore, dual-energy CT may have a role in the assessment of tumor response after several treatment methods. In a study of 27 patients with non–small cell lung cancer, the authors showed a significant decrease in the enhancement of responding metastatic lymph nodes by analyzing the data from dual-phase (arterial and venous) dual-energy chest CT examinations performed before and after chemotherapy (33). Comparison between PBV, VNC, and blended images in dual-phase dual-energy CT of the kidney was adopted to evaluate tumor response or failure to respond to radiofrequency ablation in renal cell carcinoma (34). Greater iodine distribution is seen in malignant masses on dual-energy CT images acquired

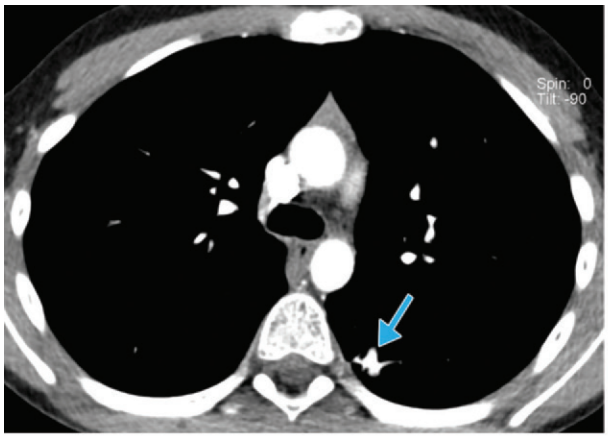

a.

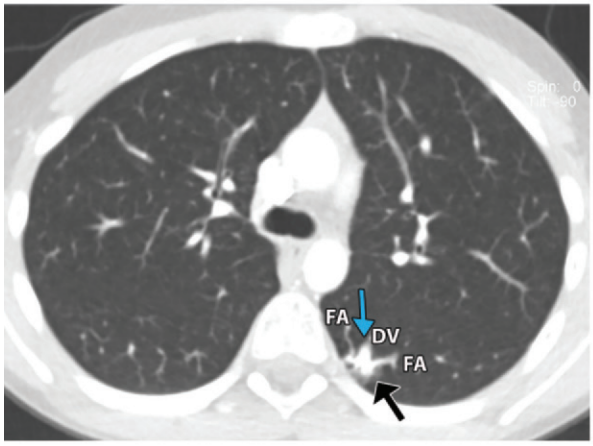

b.

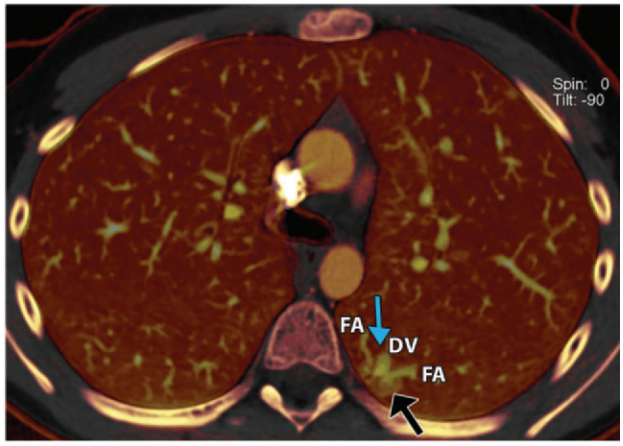

c.

Figure 6. Possible pulmonary arteriovenous malformation in a young child with a history of hereditary hemorrhagic telangiectasia and low oxygen saturation who underwent dual-energy CT protocols for pulmonary embolism. **(a, b)** Transverse CT images obtained at 60 keV show **(a)** an enhancing nodular opacity in the superior segment of the left lower lobe (arrow), with two feeding arteries *(FA)* and a draining vein *(DV)*, and **(b)** a surrounding ground-glass opacity (arrow). **(c)** Transverse PBV image shows intense iodine distribution in the superior left-lower-lobe nodular opacity, a finding compatible with arteriovenous malformation (blue arrow). High iodine distribution in the ground-glass opacity (black arrow) suggests the nidus of the arteriovenous malformation rather than pulmonary hemorrhage, scarring, or inflammation, as arteriovenous malformations usually have mildly increased iodine distribution (a light yellow color).

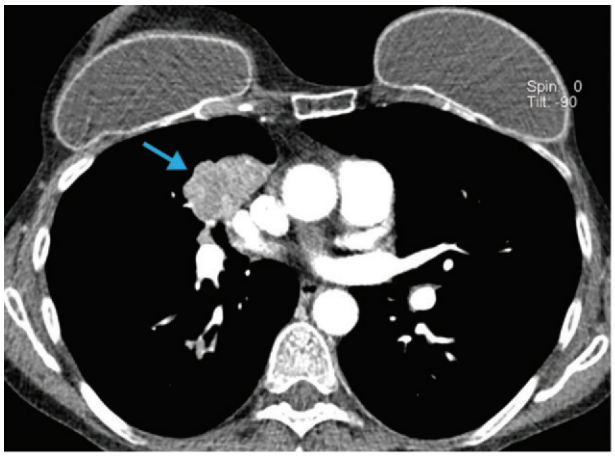

a.

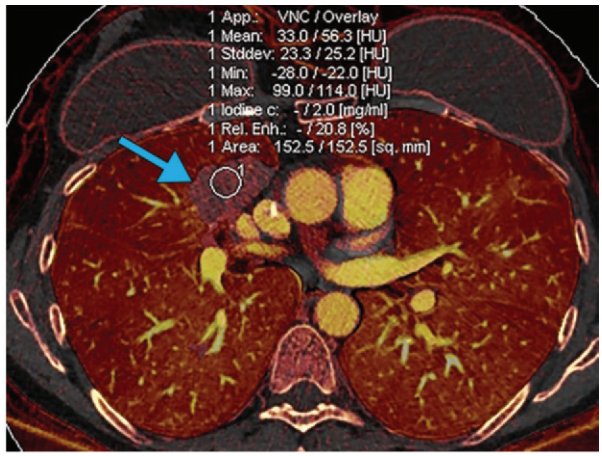

b.

Figure 7. **(a)** Routine transverse CT image obtained at 60 keV shows a central soft-tissue mass in the right upper lobe (arrow) that measures 4.3 × 3.2 cm and demonstrates heterogeneous enhancement. Note the excellent aortic and pulmonary vascular enhancement. **(b)** Transverse PBV image obtained with a 100-sec delay shows a high iodine distribution in the right-upper-lobe mass (arrow; iodine concentration, 2 mg/mL; relative enhancement , 21%), a finding that supports a malignant cause. Saline breast implants show no iodine distribution on PBV images.

at 100 seconds (Fig 7). Dual-energy CT is a good tool for assessing response to ablation procedures (Fig 8). PBV and lung analysis images can be used to assess changes in iodine redistribution (reperfusion) in the treated part of the lung.

Inflammatory Lesions of the Lung

Kim et al (35) reported different patterns of defects in iodine distribution on material decomposition images (viewed with lung analysis software) in patients with vascular and nonvascular

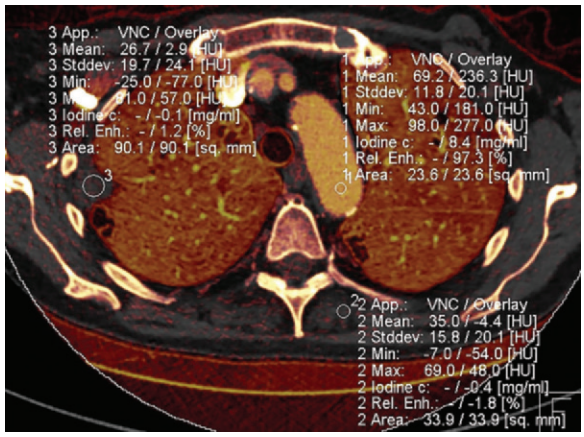

Figure 8. Quantification of iodine distribution. Transverse PBV image shows that quantification of iodine distribution can be performed by placing the region of interest in the aorta *(1)*, chest wall musculature *(2)*, and nodule *(3)*. There is negligible relative enhancement in the nodule and musculature (1.2% and –1.8%, respectively) compared with the aorta (97.3%), findings that indicate a complete response to treatment.

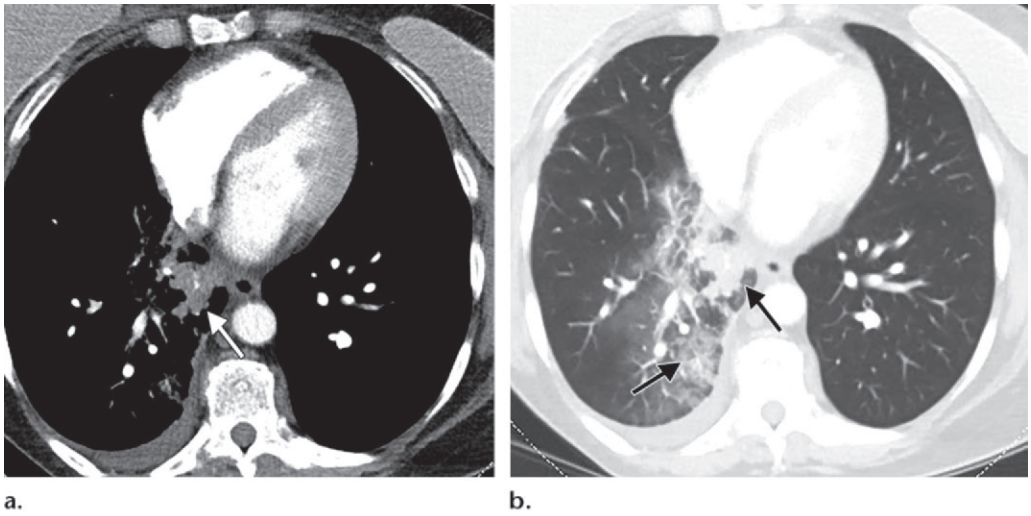

a. b.

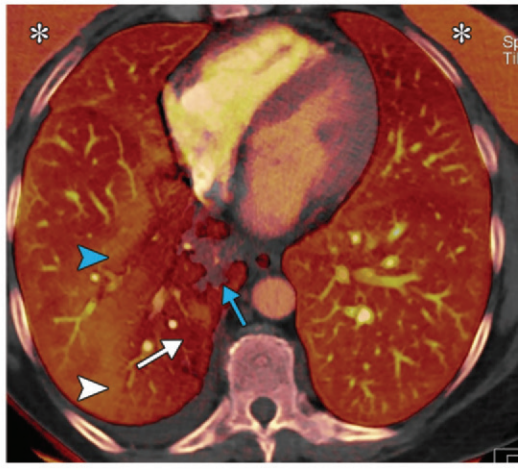

c.

Figure 9. **(a, b)** Transverse blended images show patchy mixed ground-glass and consolidative opacities in the right lower lobe (arrows). **(c)** Transverse PBV image shows heterogeneously increased iodine distribution in the region of consolidation (arrow), which is the same size as the corresponding opacity on the blended image. Low iodine distribution in the ground-glass opacities surrounds the consolidation (white arrow). A peripheral rim of increased iodine distribution may be seen and likely represents a zone of increased blood flow surrounding the area of inflammation (arrowheads). Silicone breast implants (*) are brighter on PBV images, which subtract water but not silicone.

pulmonary abnormalities who underwent dual-energy CT pulmonary angiography. A recent study of 60 patients who underwent triphasic (true unenhanced, arterial, and venous) dual-energy chest CT reported more heterogeneity in lung cancers than in inflammatory lesions. On the other hand, it was reported that there was increased enhancement in inflammatory lesions compared with neoplasms on the basis of attenuation values and iodine concentration on monochromatic 70-keV and PBV images, respectively (36). In contrast to pulmonary infarctions, which demonstrate homogeneous low iodine distribution on iodine or PBV images, pneumonia demonstrates heterogeneously decreased or increased iodine distribution (Fig 9). Homogeneously increased iodine distribution occurs in atelectasis (Fig 10). In pneumonia and atelectasis, the abnormalities seen on PBV and conventional lung images are of the same size but have greater mismatch in infarcts. Thus, differentiation from pulmonary infarction requires comparison of the

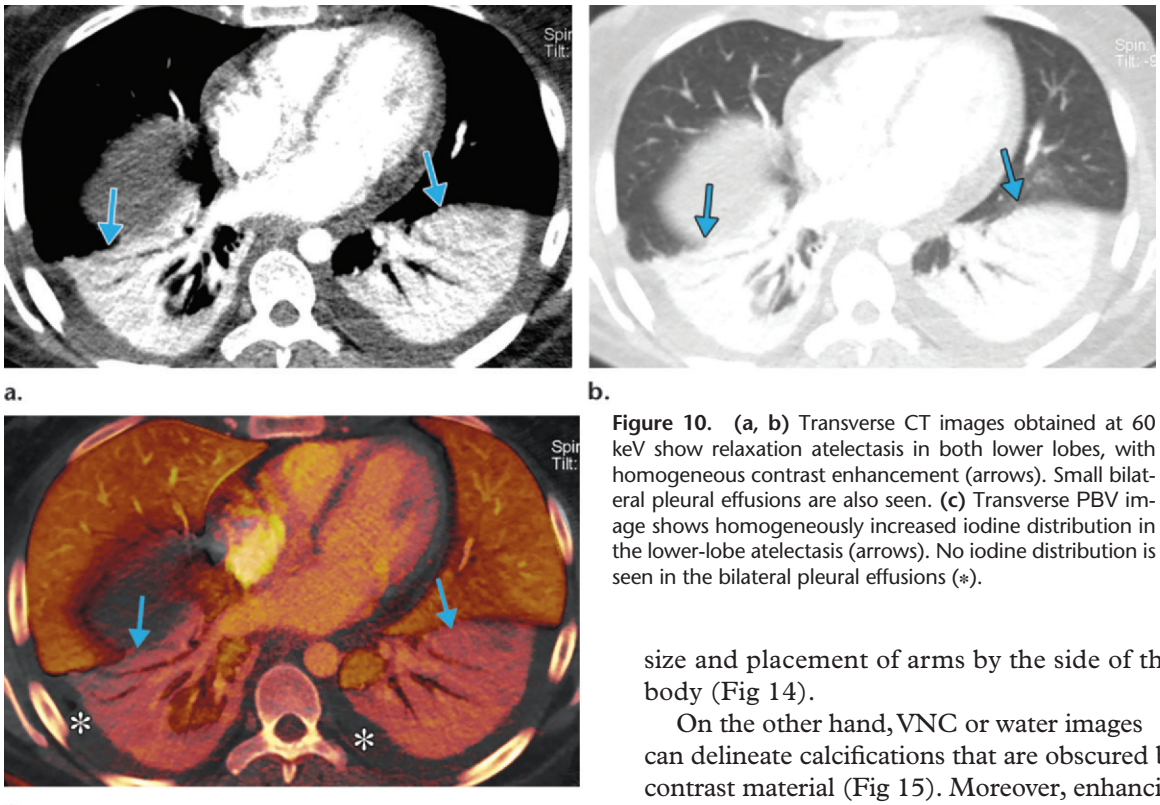

Figure 10. **(a, b)** Transverse CT images obtained at 60 keV show relaxation atelectasis in both lower lobes, with homogeneous contrast enhancement (arrows). Small bilateral pleural effusions are also seen. **(c)** Transverse PBV image shows homogeneously increased iodine distribution in the lower-lobe atelectasis (arrows). No iodine distribution is seen in the bilateral pleural effusions (*).

size of the opacity with the size of the PBV abnormality in the setting of a positive pulmonary embolism at dual-energy CT. Lung abscess and other necrotic lung lesions do not demonstrate iodine distribution on PBV images (Fig 11).

Airways Disease

The use of xenon as an inhalational contrast agent for dual-energy CT can allow qualitative and quantitative assessment of lung ventilation. The extent of ventilation defects at xenon inhalation dual-energy CT in patients with bronchial asthma shows a good correlation with pulmonary function tests (37). Likewise, changes in airflow after the administration of bronchodilators can also be assessed with dual-energy CT (38).

A synchronous interpretation of conventional attenuation-contrast and PBV images is necessary to differentiate among PBV defects that result from diseases such as emphysema and air trapping (39) (Fig 12). Because of the lack of iodine distribution, air-filled bronchiectasis and honeycombing are easily identified on PBV images (Fig 13).

Miscellaneous Applications

The ability of dual-energy CT to reduce metal or contrast agent–related streak artifacts has been well documented in the literature (40,41). Creation of higher-kilovoltage images can help troubleshoot artifacts related to large patient size and placement of arms by the side of the body (Fig 14).

On the other hand, VNC or water images can delineate calcifications that are obscured by contrast material (Fig 15). Moreover, enhancing lymph nodes can be distinguished from nodes that contain calcium, silica, or magnesium on VNC images, a characteristic that is important in identifying residual tumor and inflammatory processes.

Furthermore, silicone and saline breast implants have different attenuation on material decomposition images: Whereas silicone implants have an intense or bright appearance on PBV or iodine images, saline implants have low attenuation (Figs 7, 9). On the basis of this fact, there is potential for dual-energy CT to depict ruptured silicone implants similar to manner in which magnetic resonance imaging does (42). Further studies with large sample sizes are necessary to confirm this indication.

Strengths and Limitations

There is a growing list of applications for dual-energy CT of the chest. In addition to the applications already discussed, dual-energy CT has also been used to correct for certain metal artifacts. Improved contrast enhancement, particularly on lower-kilovoltage images, can allow reduction of the total volume of contrast material given to patients.

On the other hand, a review of the extra images generated from dual-energy CT (eg, blended, monoenergetic, maximum intensity projection, sagittal, and coronal) can increase the interpretation time. Contrast streak and cardiac and diaphragmatic motion artifacts can impair material decomposition images. Radiation dose considerations were described in a separate section.

a.

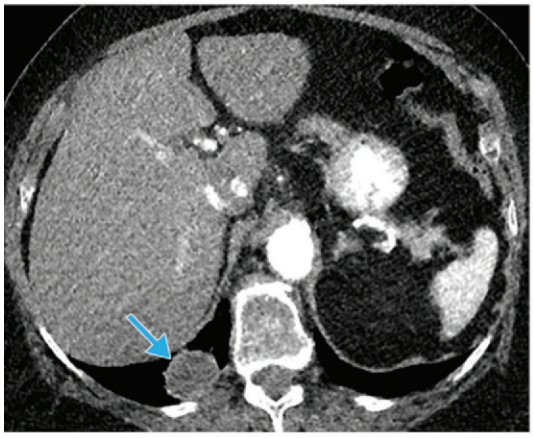

b.

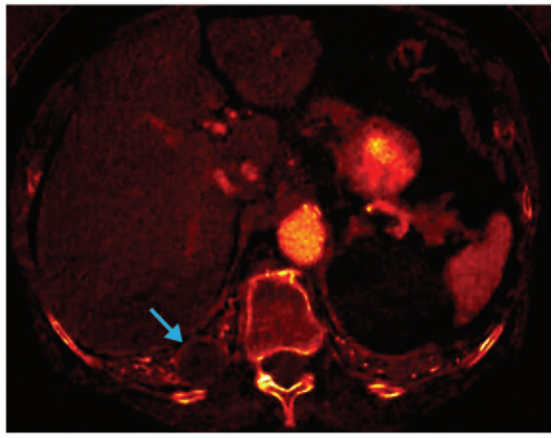

c.

Figure 11. **(a)** Transverse VNC image shows a well-defined 3.4-cm mass (arrow) in the right lower lobe. **(b)** Transverse CT image obtained at 60 keV shows a lack of substantial enhancement in the right-lower-lobe mass (arrow). **(c)** Transverse PBV image shows a low distribution of iodine in the right-lower-lobe mass (arrow), a finding that supports a benign cause and was confirmed at tissue sampling, which confirmed the diagnosis of lung abscess.

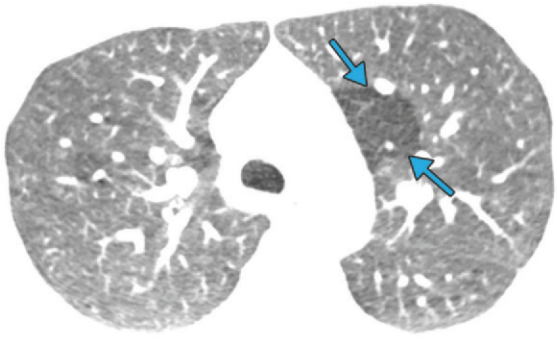

a.

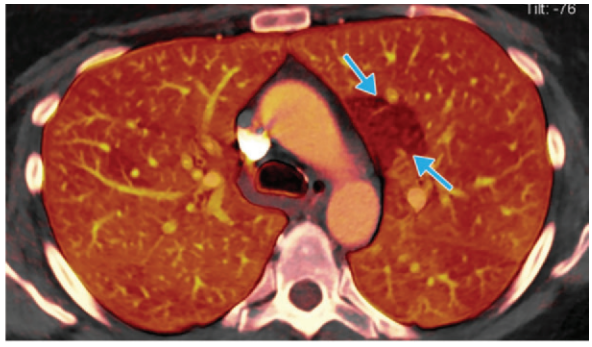

b.

Figure 12. **(a)** Transverse CT image obtained at 60 keV shows an area of low attenuation (arrows) in the left upper lobe. **(b)** PBV image shows a corresponding area of homogeneously decreased iodine distribution (arrows), a finding that suggests a matching defect of air trapping. In vascular PBV defects, a mismatched defect is seen on PBV images.

Conclusion

Common thoracic conditions have distinct features at dual-energy CT; therefore, the use of dual-energy CT enhances diagnostic confidence without substantial radiation penalties. In addition, the use of dual-energy CT allows a reduction in contrast material volume, contrast material– and metal-related beam hardening artifacts, and artifacts related to body parts.

References

1. Yu L, Leng S, McCollough CH. Dual-energy CT-based monochromatic imaging. AJR Am J Roentgenol 2012;199(5 Suppl):S9–S15.
2. Kang MJ, Park CM, Lee CH, Goo JM, Lee HJ. Dual-energy CT: clinical applications in various pulmonary diseases. RadioGraphics 2010;30(3):685–698.
3. Kraśnicki T, Podgórski P, Guziński M, et al. Novel clinical applications of dual energy computed tomography. Adv Clin Exp Med 2012;21(6):831–841.
4. Lira D, Padole A, Kalra MK, Singh S. Tube potential and CT radiation dose optimization. AJR Am J Roentgenol 2015;204(1):W4–W10.
5. Bushberg JT. The AAPM/RSNA physics tutorial for residents. X-ray interactions. RadioGraphics 1998;18(2):457–468.

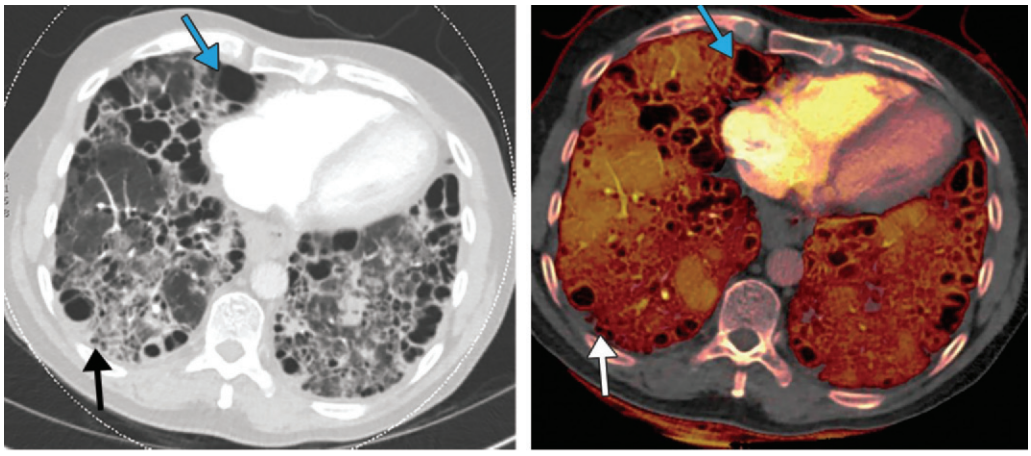

a. b.

Figure 13. Pulmonary fibrosis in a 67-year-old man with a history of interstitial lung disease who underwent dual-energy CT with pulmonary embolism protocols. **(a)** Transverse CT image obtained at 60 keV shows diffuse honeycombing (black arrow) and bronchiectasis (blue arrow), findings consistent with pulmonary fibrosis. **(b)** Transverse PBV image shows heterogeneous iodine distribution, with no iodine distribution in the areas of architectural distortion and cystic change (arrows).

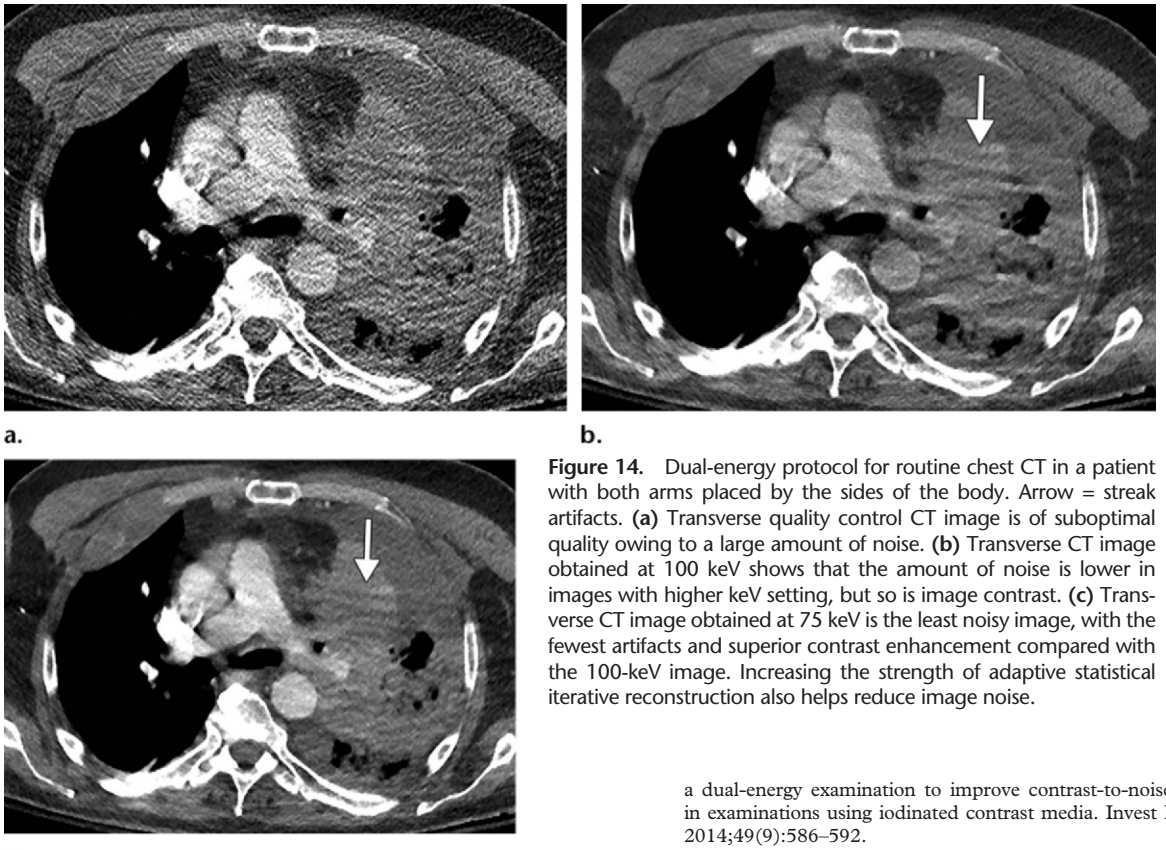

a. b. c.

Figure 14. Dual-energy protocol for routine chest CT in a patient with both arms placed by the sides of the body. Arrow = streak artifacts. **(a)** Transverse quality control CT image is of suboptimal quality owing to a large amount of noise. **(b)** Transverse CT image obtained at 100 keV shows that the amount of noise is lower in images with higher keV setting, but so is image contrast. **(c)** Transverse CT image obtained at 75 keV is the least noisy image, with the fewest artifacts and superior contrast enhancement compared with the 100-keV image. Increasing the strength of adaptive statistical iterative reconstruction also helps reduce image noise.

6. Johnson TR. Dual-energy CT: general principles. AJR Am J Roentgenol 2012;199(5 Suppl):S3–S8.
7. Agrawal MD, Pinho DF, Kulkarni NM, Hahn PF, Guimaraes AR, Sahani DV. Oncologic applications of dual-energy CT in the abdomen. RadioGraphics 2014;34(3):589–612.
8. Ginat DT, Gupta R. Advances in computed tomography imaging technology. Annu Rev Biomed Eng 2014;16:431–453.
9. Grant KL, Flohr TG, Krauss B, Sedlmair M, Thomas C, Schmidt B. Assessment of an advanced image-based technique to calculate virtual monoenergetic computed tomographic images from a dual-energy examination to improve contrast-to-noise ratio in examinations using iodinated contrast media. Invest Radiol 2014;49(9):586–592.
10. Singh S, Kalra MK. Standardized CT protocols and nomenclature: better, but not yet there. Pediatr Radiol 2014;44(Suppl 3):440–443.
11. Mayo J, Thakur Y. Pulmonary CT angiography as first-line imaging for PE: image quality and radiation dose considerations. AJR Am J Roentgenol 2013;200(3):522–528.
12. Bauer RW, Kramer S, Renker M, et al. Dose and image quality at CT pulmonary angiography-comparison of first and second generation dual-energy CT and 64-slice CT. Eur Radiol 2011;21(10):2139–2147.
13. Purysko AS, Primak AN, Baker ME, et al. Comparison of radiation dose and image quality from single-energy and dual-energy CT examinations in the same patients screened for hepatocellular carcinoma. Clin Radiol 2014;69(12):e538–e544.

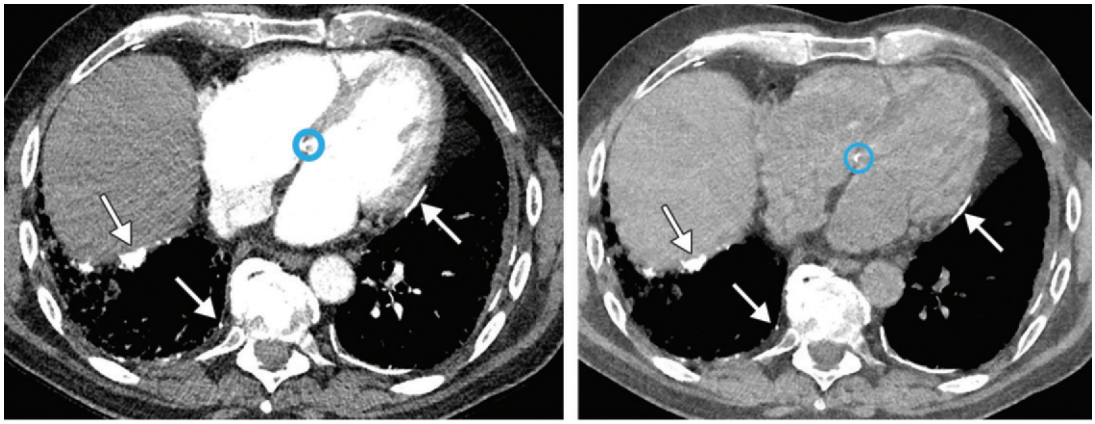

a. b.

Figure 15. **(a)** Transverse contrast-enhanced CT image obtained at 60 keV shows bilateral calcified pleural plaques (arrows), a finding consistent with previous asbestos exposure. Circle = interventricular septum. **(b)** Transverse VNC image shows bilateral calcified pleural plaques (arrows) and calcification in the interventricular septum (circle), a finding that was obscured at contrast-enhanced CT.

14 Apfaltrer P, Sudarski S, Schneider D, et al. Value of monoenergetic low-kV dual energy CT datasets for improved image quality of CT pulmonary angiography. Eur J Radiol 2014;83(2):322–328.
15. ACR manual on contrast media. Version 9. American College of Radiology. http://www.acr.org/quality-safety/resources/~/media/37D84428BF1D4E1B9A3A2918DA9E27A3.pdf/. Published 2013. Accessed DATE.
16. Delesalle MA, Pontana F, Duhamel A, et al. Spectral optimization of chest CT angiography with reduced iodine load: experience in 80 patients evaluated with dual-source, dual-energy CT. Radiology 2013;267(1):256–266.
17. Kerl JM, Bauer RW, Renker M, et al. Triphasic contrast injection improves evaluation of dual energy lung perfusion in pulmonary CT angiography. Eur J Radiol 2011;80(3):e483–e487.
18. Geyer LL, Scherr M, Körner M, et al. Imaging of acute pulmonary embolism using a dual energy CT system with rapid kVp switching: initial results. Eur J Radiol 2012;81(12):3711–3718.
19. Lu GM, Zhao Y, Zhang LJ, Schoepf UJ. Dual-energy CT of the lung. AJR Am J Roentgenol 2012;199(5 Suppl):S40–S53.
20. Mettler FA Jr, Guiberteau MJ. Respiratory system. In: Essentials of nuclear medicine imaging. 6th ed. Philadelphia, Pa: Elsevier Saunders, 2012; 195–236.
21. Shenoy V, Anton JM, Collard CD, Youngblood SC. Pulmonary thromboendarterectomy for chronic thromboembolic pulmonary hypertension. Anesthesiology 2014;120(5):1255–1261.
22. Ameli-Renani S, Rahman F, Nair A, et al. Dual-energy CT for imaging of pulmonary hypertension: challenges and opportunities. RadioGraphics 2014;34(7):1769–1790.
23. Dournes G, Verdier D, Montaudon M, et al. Dual-energy CT perfusion and angiography in chronic thromboembolic pulmonary hypertension: diagnostic accuracy and concordance with radionuclide scintigraphy. Eur Radiol 2014;24(1):42–51.
24. Ameli-Renani S, Ramsay L, Bacon JL, et al. Dual-energy computed tomography in the assessment of vascular and parenchymal enhancement in suspected pulmonary hypertension. J Thorac Imaging 2014;29(2):98–106.
25. Godoy MC, Naidich DP, Marchiori E. Single-acquisition dual-energy multidetector computed tomography: analysis of vascular enhancement and postprocessing techniques for evaluating the thoracic aorta. J Comput Assist Tomogr.
26. Stolzmann P, Frauenfelder T, Pfammatter T, et al. Endoleaks after endovascular abdominal aortic aneurysm repair: detection with dual-energy dual-source CT. Radiology 2008;249(2):682–691.
27. Numburi UD, Schoenhagen P, Flamm SD, et al. Feasibility of dual-energy CT in the arterial phase: Imaging after endovascular aortic repair. AJR Am J Roentgenol 2010;195(2):486–493.
28. Lee SH, Hur J, Kim YJ, Lee HJ, Hong YJ, Choi BW. Additional value of dual-energy CT to differentiate between benign and malignant mediastinal tumors: an initial experience. Eur J Radiol 2013;82(11):2043–2049.
29. Schmid-Bindert G, Henzler T, Chu TQ, et al. Functional imaging of lung cancer using dual energy CT: how does iodine related attenuation correlate with standardized uptake value of 18FDG-PET-CT? Eur Radiol 2012;22(1):93–103.
30. Chae EJ, Song JW, Seo JB, Krauss B, Jang YM, Song KS. Clinical utility of dual-energy CT in the evaluation of solitary pulmonary nodules: initial experience. Radiology 2008;249(2):671–681.
31. De Cecco CN, Darnell A, Rengo M, et al. Dual-energy CT: oncologic applications. AJR Am J Roentgenol 2012;199(5 Suppl):S98–S105.
32. Yang Y, Jia X, Deng Y, Chen J, Zhang LJ. Can virtual non-enhanced CT be used to replace true non-enhanced CT for the detection of palpable cervical lymph nodes? A preliminary study. Jpn J Radiol 2014;32(6):324–330.
33. Baxa J, Vondráková A, Matoušková T, et al. Dual-phase dual-energy CT in patients with lung cancer: assessment of the additional value of iodine quantification in lymph node therapy response. Eur Radiol 2014;24(8):1981–1988.
34. Park SY, Kim CK, Park BK. Dual-energy CT in assessing therapeutic response to radiofrequency ablation of renal cell carcinomas. Eur J Radiol 2014;83(2):e73–e79.
35. Kim BH, Seo JB, Chae EJ, Lee HJ, Hwang HJ, Lim C. Analysis of perfusion defects by causes other than acute pulmonary thromboembolism on contrast-enhanced dual-energy CT in consecutive 537 patients. Eur J Radiol 2012;81(4):e647–e652.
36. Hou WS, Wu HW, Yin Y, Cheng JJ, Zhang Q, Xu JR. Differentiation of lung cancers from inflammatory masses with dual-energy spectral CT imaging. Acad Radiol 2015;22(3):337–344.
37. Kim WW, Lee CH, Goo JM, et al. Xenon-enhanced dual-energy CT of patients with asthma: dynamic ventilation changes after methacholine and salbutamol inhalation. AJR Am J Roentgenol 2012;199(5):975–981.
38. Chae EJ, Seo JB, Lee J, et al. Xenon ventilation imaging using dual-energy computed tomography in asthmatics: initial experience. Invest Radiol 2010;45(6):354–361.
39. Ferda J, Ferdová E, Mírka H, et al. Pulmonary imaging using dual-energy CT, a role of the assessment of iodine and air distribution. Eur J Radiol 2011;77(2):287–293.
40. Wang Y, Qian B, Li B, et al. Metal artifacts reduction using monochromatic images from spectral CT: evaluation of pedicle screws in patients with scoliosis. Eur J Radiol 2013;82(8):e360–e366.
41. Pessis E, Campagna R, Sverzut JM, et al. Virtual monochromatic spectral imaging with fast kilovoltage switching: reduction of metal artifacts at CT. RadioGraphics 2013;33(2):573–583.
42. Johnson TR, Himsl I, Hellerhoff K, et al. Dual-energy CT for the evaluation of silicone breast implants. Eur Radiol 2013;23(4):991–996.